Clim Dyn (2015) 44:1627–1644
DOI 10.1007/s00382-014-2453-5

Using nudging to improve global-regional dynamic consistency in limited-area climate modeling: What should we nudge?

Hiba Omrani · Philippe Drobinski · Thomas Dubos

Received: 31 October 2013 / Accepted: 13 December 2014 / Published online: 9 January 2015

Abstract Regional climate modelling sometimes requires that the regional model be nudged towards the large-scale driving data to avoid the development of inconsistencies between them. These inconsistencies are known to produce large surface temperature and rainfall artefacts. Therefore, it is essential to maintain the synoptic circulation within the simulation domain consistent with the synoptic circulation at the domain boundaries. Nudging techniques, initially developed for data assimilation purposes, are increasingly used in regional climate modeling and offer a workaround to this issue. In this context, several questions on the "optimal" use of nudging are still open. In this study we focus on a specific question which is: What variable should we nudge? in order to maintain the consistencies between the regional model and the driving fields as much as possible. For that, a "Big Brother Experiment", where a reference atmospheric state is known, is conducted using the weather research and forecasting (WRF) model over the Euro–Mediterranean region. A set of 22 3-month simulations is performed with different sets of nudged variables and nudging options (no nudging, indiscriminate nudging, spectral nudging) for summer and winter. The results show that nudging clearly improves the model capacity to reproduce the reference fields. However the skill scores depend on the set of variables used to nudge the regional climate simulations. Nudging the tropospheric horizontal wind is by far the key variable to nudge to simulate correctly surface temperature and wind, and rainfall. To a lesser extent, nudging tropospheric temperature also contributes to significantly improve the simulations. Indeed, nudging tropospheric wind or temperature directly impacts the simulation of the tropospheric geopotential height and thus the synoptic scale atmospheric circulation. Nudging moisture improves the precipitation but the impact on the other fields (wind and temperature) is not significant. As an immediate consequence, nudging tropospheric wind, temperature and moisture in WRF gives by far the best results with respect to the Big-Brother simulation. However, we noticed that a residual bias of the geopotential height persists due to a negative surface pressure anomaly which suggests that surface pressure is the missing quantity to nudge. Nudging the geopotential has no discernible effect. Finally, it should be noted that the proposed strategy ensures a dynamical consistency between the driving field and the simulated small-scale field but it does not ensure the best "observed" fine scale field because of the possible impact of incorrect driving large-scale field.

Keywords Regional climate modeling · Nudging · Big Brother Experiment · WRF model

1 Introduction

Dynamical down-scaling has been widely used to improve regional climate description at fine scale. It consists in driving a regional climate model (RCM) by large-scale fields provided by a global circulation model (GCM) or (re) analysis as initial and boundary conditions. Previous studies (e.g. Miguez-Macho et al. 2004; Lo et al. 2008; Radu et al. 2008; Salameh et al. 2010) have shown the necessity of relaxing the three-dimensional RCM fields towards the GCM fields to avoid deviation from the large-scale atmospheric circulation. This relaxation technique, also referred

H. Omrani (✉) · P. Drobinski · T. Dubos
Laboratoire de Météorologie Dynamique, CNRS,
Institut Pierre Simon Laplace, Ecole Polytechnique,
91128 Palaiseau Cedex, France
e-mail: hiba.omrani@lmd.polytechnique.fr

to as nudging, consists in partially imposing the large scale of the driving fields provided by global climate models (GCM) or (re)-analyses, on the regional climate model (RCM) simulation with the aim of disallowing large and unrealistic departures between driving and driven fields. Two different types of nudging exist, indiscriminate nudging (IN), also referred to as data assimilation, dynamical relaxation, grid-point nudging or analysis nudging, consists in driving the RCM indiscriminately at all scales (Davies and Turner 1977; Stauffer and Seaman 1990; Lo et al. 2008; Salameh et al. 2010; Omrani et al. 2012a). Spectral nudging (SN) consists in driving the RCM on selected spatial scales only (e.g. Kida et al. 1991; Waldron et al. 1996; von Storch et al. 2000; Radu et al. 2008; Omrani et al. 2012b).

Nudging was initially developed for data assimilation purposes. Several studies have investigated the "optimal" use of nudging by varying nudging parameters (Zou et al. 1992; Stauffer and Bao 1993; Vidard et al. 2003; Lei et al. 2012). The first motivation of using nudging in data assimilation is to minimize the model errors with respect to observations or gridded analysis, whereas, nudging is used in regional climate modeling to ensure a dynamical consistency between the driving field and the simulated large-scale fields, however it does not ensure the best observed fine scale field because of the possible impact of incorrect driving large-scale field. In this context, the optimal nudging strategies with respect to dynamic downscaling could add skill whenever the parent global model has some level of skill.

Nudging can be applied to a different set of meteorological variables depending on models, nudging technique (IN or SN) and the down-scaling purpose (see Table 1). However, how to choose the nudged variable(s) remains an open question. Only few studies have addressed this issue. Radu et al. (2008) analyzed the sensitivity of RCM simulations to the nudged variables in order to quantify the associated uncertainties. Recently Pohl and Crétat (2013) explored the impact of the nudged variables on the WRF simulated deep atmospheric convection in the tropics. They showed that nudging temperature reduces the model bias, while nudging horizontal wind improves the model time variability with respect to the observations. In the present work, we adopt an idealized approach known as the Big Brother Experiment (BBE) (Denis et al. 2002a) in order to evaluate the "best" set of variables to be nudged and the physical processes supporting such optimal configuration, if they exist. However, the variables that can be nudged differ between models and between indiscriminate and spectral nudging (Table 1). The WRF model is thus chosen here because of the possibility to apply both indiscriminate and spectral nudging techniques all other things being equal, and as a natural follow-up of Omrani et al. (2013). To isolate the effect of nudging without any interference with other sources of error and uncertainty propagation, a BBE approach is used as in Omrani et al. (2013), meaning that the same model and hence the same physics are used between the driving and driven models. Indeed, in real regional climate modeling, the GCM used to drive the RCM have generally different numerical schemes and physical parameterizations (e.g. Kanamaru and Kanamitsu 2007; Thatcher and McGregor 2009). In addition, the validation of regional climate simulations must eventually

Table 1 Review of variables used for nudging in various models

Model	Nudging technique	Nudged variables	References
MM5	IN	u, v, T, q, ζ	Stauffer and Seaman (1990)
RAMS	SN	u, v, θ_{il}, π'	Miguez-Macho et al. (2004)
CRCM	SN	u, v	De Elia et al. (2008)
CRCM	SN	u, v	Alexandru et al. (2009)
CLM	SN	u, v	Rockel et al. (2008)
WRF	IN	u, v, θ, q	Lo et al. (2008)
MM5	IN	u, v, θ, h, sm	Otte (2008a, b)
ARPEGE/ALADIN	SN	T, p_s, h, div, ω	Radu et al. (2008)
WRF	IN	u, v, θ, q	Bowden et al. (2012)
WRF	SN	u, v, θ, Φ	Bowden et al. (2012)
WRF	IN, obs nudging	u, v, θ, q	Rogers et al. (2013)
WRF	IN	u, v, θ, q	Omrani et al. (2013)
WRF	SN	u, v, θ, Φ	Omrani et al. (2013)

The reference in which the model nudging configuration is given in the left column. The model as well as the nudging technique used in the cited reference are given in the second and third column from left, respectively. The right column details the variables used for nudging. The quantities $T, u, v, \theta, \theta_{il}, \pi', h, q, p_s, div, \omega, \zeta, \Phi$ refer to temperature, zonal wind, meridional wind, potential temperature, modified equivalent potential temperature that is conserved in both ice-to-liquid and liquid-to-vapor, Exner function perturbation, specific humidity, water vapor mixing ratio, surface pressure, divergence, vorticity and geopotentail height, respectively

be done by comparing to observations, often using gridded datasets like CRU and ECA&D which have their own uncertainties and biases (Flaounas et al. 2012).

For all these reasons, it must be clear that the ideal nudging configuration of WRF discussed in this study may not at the end produce the best results due to other uncertainty sources. However, it offers a set of controlled experiments designed to isolate the impact of nudging one variable rather than another and to understand the different physical processes involved.

This paper is organized as follows. A description of the WRF model and the experimental set-up is given in Sect. 2. In Sect. 3 we quantify statistically the impact of the different sets of nudged variables on the simulation of fields of great importance for regional climate modeling: surface temperature, wind and rainfall. Potential dynamical processes causes for the different responses observed are analyzed and discussed in Sect. 4. Finally, Sect. 5 summarizes the results and points out some open research questions needing further investigation.

2 The model and the experiment design

The model used in this study is the 3.1.1 version of the weather research and forecasting model (WRF) released on July 31, 2009. WRF is a limited area model, non-hydrostatic, with terrain following sigma-coordinate mesoscale modeling system designed to serve both operational forecasting and atmospheric research needs (Skamarock and Klemp 2007). The WRF development is a collaborative partnership, principally among the National Center for Atmospheric Research (NCAR), the National Oceanic and Atmospheric Administration (the National Centers for Environmental Prediction (NCEP) and the Earth System Research Laboratory (ESRL), the Air Force Weather Agency (AFWA), the Naval Research Laboratory, the University of Oklahoma, and the Federal Aviation Administration (FAA). WRF offers a flexible and robust platform not only used but also developed by a worldwide research community including government laboratories, academia and the private sector.

The physical options chosen to perform the simulations include the WRF Single-Moment 5-class microphysical parameterization (Hong and Juang 1998; Hong et al. 2004), the new Kain–Fritsch convective parameterization (Kain 2004), the Dudhia shortwave radiation (Dudhia 1989) and Rapid Radiative Transfer Model longwave radiation (Mlawer et al. 1997) and the Yonsei University planetary boundary layer scheme (Hong et al. 2006). For the land surface model, a 5-layer diffusive scheme is used here.

As in Omrani et al. (2013), we conduct a "Big-Brother Experiment". It consists in first establishing a reference climate by performing a large-domain high-resolution RCM simulation: this simulation is called the Big-Brother (BB). This reference simulation is then degraded by filtering short scales that are generally unresolved by the driving fields (DF) (e.g. global reanalysis and global climate models). This filtered reference is then used to drive the same nested RCM (called the Little-Brother LB), integrated at the same high-resolution as the Big Brother, but over a smaller domain that is embedded in the Big-Brother domain. The climate statistics of the Little Brother are then compared with those of the Big-Brother over the Little-Brother domain (Fig. 1). Differences can thus be attributed easily to errors associated with the downscaling technique, and not to model errors nor to observation limitations.

2.1 Nudging

We investigate the two existing nudging techniques in WRF, i.e. the indiscriminate nudging (IN) (Stauffer and Seaman 1990) and the spectral nudging (SN) (Cha et al. 2006). The nudging technique consists in relaxing the model state towards the driving large-scale fields by adding a non-physical term to the model equation. This nudging term is defined as the difference between the observation and the model solution weighted by a nudging coefficient which is the inverse of the nudging time τ. In WRF, indiscriminate nudging is represented by the general following equation described by Stauffer and Seaman (1990) [Eq. (1)].

$$\frac{\partial p^* \alpha_{LB}}{\partial t} = F(\alpha_{LB}, x, t) + \frac{1}{\tau} W(x,t)\, \epsilon(x)\, p^* (\alpha_{DF} - \alpha_{LB}) \quad (1)$$

where α is a prognostic variable, $p^* = p_s - p_t$ is a mass-weighting factor due to the use of a terrain-following sigma-coordinate, $p_t = 50\,\text{hPa}$ is the pressure at the model top, p_s is the surface pressure, x represents the spatial variables, t is time. The model's physical forcing terms (advection, Coriolis effects, etc.) are represented by F. The subscripts DF and LB stand for driving field and Little-Brother, respectively. The quantity $1/\tau$ is the nudging coefficient, with τ a relaxation time scale for the nudging term. The nudging coefficient can vary in time and space with a four-dimensional weighting function W. Finally, ϵ is the analysis quality factor which ranges between 0 and 1.

In WRF, indiscriminate nudging can be applied to the wind components u and v (u and v are grid-relative wind components but in this study with the Mercator projection u and v are the zonal and meridional wind components, respectively), to the potential temperature θ, and to the water vapor mixing ratio q. Nudging can be restricted to not act within the atmospheric boundary layer or below a user-specified model level (Rogers et al. 2013). For indiscriminate nudging, Omrani et al. (2012a) show that the smaller

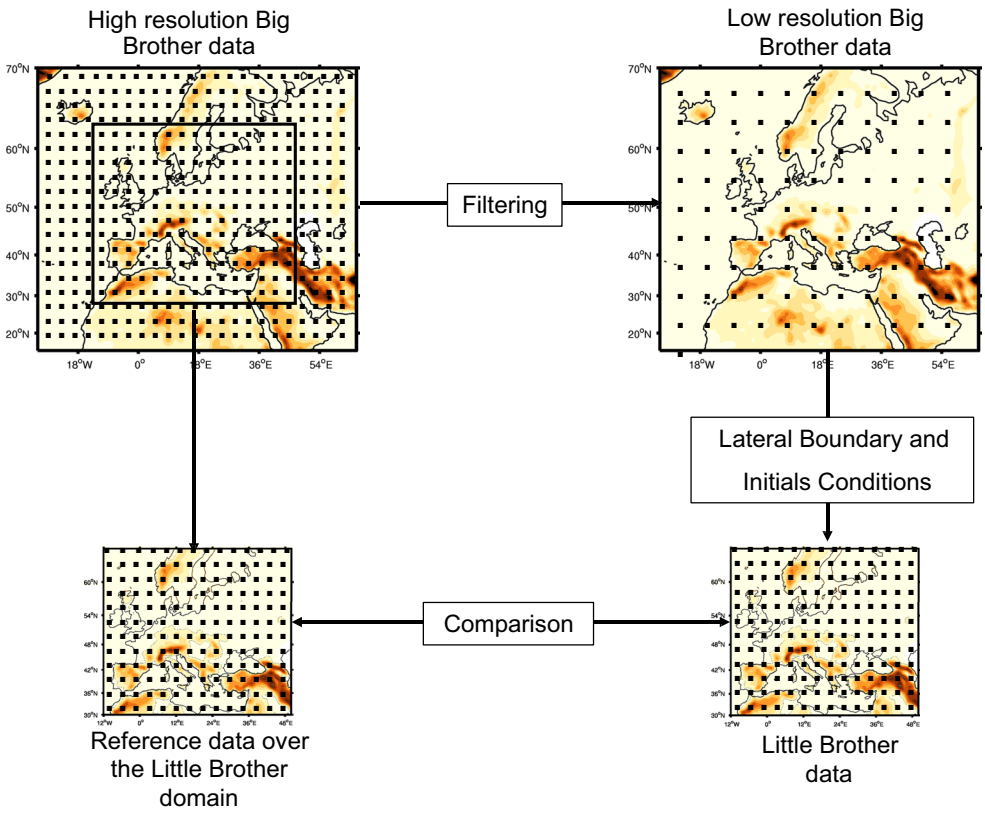

Fig. 1 "Big-Brother" experiment diagram using a limited area model (LAM) as a regional climate model (RCM)

the nudging time τ, the closer the RCM predictions α_{LB} to the driving fields α_{DF} interpolated on the RCM grid and the larger the inhibition of the small-scale RCM dynamics.

The spectral nudging technique technique consists in driving the RCM on selected spatial scales only and does not affect the small-scale fields since only the large scales are relaxed. In this study, the cutoff wavelength corresponds to 300 km. Spectral nudging in WRF can be applied to the wind components, potential temperature and geopotential Φ. The spectral nudging equation is that of Miguez-Macho et al. (2004):

$$\frac{\partial \alpha_{LB}}{\partial t} = L(\alpha_{LB}) + \sum_{|n|\leq N} \sum_{|m|\leq M} \frac{1}{\tau_{mn}} \left(\alpha_{mn}^{DF} - \alpha_{mn}^{LB}\right) e^{ik_m x} e^{ik_n y} \quad (2)$$

where α represents the prognostic variable being nudged, L is the model operator, α_{mn}^{DF} and α_{mn}^{LB} represent the spectral coefficients of α_{DF} and α_{LB}. The nudging coefficient $\frac{1}{\tau_{mn}}$ can vary with m and n (wavenumbers in the x and y direction, respectively) as well as height; k_m and k_n then represent the wave vector and are dependent on the domain size, D_x and D_y, given by:

$$k_m = \frac{2\pi\, m}{D_x} \quad \text{and} \quad k_n = \frac{2\pi\, n}{D_y}$$

Following Lo et al. (2008), the nudging term is applied only above the planetary boundary layer (PBL) with a time-dependent height diagnosed by the planetary boundary layer scheme. In fact, nudging in the PBL may prevent reasonable mesoscale structures from being developed by constraining these structures toward large-scale driving fields. Above that height the nudging coefficient is constant. The nudging coefficient can be defined separately for each nudged variable, however in this work we use the same nudging coefficient for all the nudged variables. It is set to six hours (6 h). This time defined as "the optimal nudging time" was determined in Omrani et al. (2013) using the same model configuration, where a set of experiment was conducted by varying the nudging times (01, 03, 06 and 12 h). However, it should be noticed that the "optimal" nudging time used here is not universal but depends on the model configuration.

2.2 Simulations

A set of 2 × 11 simulations has been performed for winter and summer by varying the set of nudged variables, for both indiscriminate and spectral nudging techniques (Table 2). The BB simulation was performed over a large domain covering Europe and North Africa (Fig. 1) with 130 × 140

horizontal grid points with a 50 km horizontal resolution, as required within CORDEX (Giorgi et al. 2009), and 28 vertical levels. The model top is at 50 hPa. The winter simulations start on 1 December 1989 to 28 February 1990 with one month spin up (November 1989). The summer simulations start on 1 June 1990 to 31 August 1990 with one month spin up (May 1990). The initial and boundary conditions of the BB simulation are provided by the ERA-Interim reanalysis of the European Center for Medium-range Weather Forecast (ECMWF). The resolution of the BB fields are then degraded using a simple low pass averaging filter to obtain a resolution of 300 km × 300 km from the 50 km × 50 km fields and to serve as large-scale driving fields for the LB simulations.

The LB simulations have been performed with a 50 km resolution over the EURO-CORDEX domain (98 × 100 horizontal grid points) covering Europe and the Mediterranean regions (Fig. 1). When indiscriminate or spectral nudging is used, it is applied above the planetary boundary layer as suggested by Lo et al. (2008). The variables that can be nudged are the potential temperature, wind and moisture for IN and the potential temperature, wind and geopotential for SN. The update frequency of the large-scale driving fields is set to 6 h since the ERA-Interim reanalyses and CMIP5 climate simulations used in the frame of HyMeX (Drobinski et al. 2009) and MED-CORDEX programs are also sampled every 6 h. WRF automatically performs a linear time interpolation between two samples of the driving fields.

To quantify the ability of the LB to reproduce the reference field, we use the mean bias δ, the root mean square error ε, the standard deviation σ and the correlation coefficient γ.

Table 2 List of performed simulations

Experiment name	Nudging technique	Nudged variables
NN	No nudging	None
IN-All	Indiscriminate	θ, u, v, q
IN-UV	Indiscriminate	u, v
IN-T	Indiscriminate	θ
IN-Q	Indiscriminate	q
IN-UV&T	Indiscriminate	θ, u, v
IN-UV&Q	Indiscriminate	u, v, q
IN-T&Q	Indiscriminate	θ, q
SN-All	Spectral	$\theta, u, v,$
SN-UV	Spectral	u, v
SN-T	Spectral	θ
SN-Φ	Spectral	Φ
SN-UV&Φ	Spectral	u, v, Φ
SN-T&Φ	Spectral	θ, Φ

3 Sensitivity analysis to the nudged variables

In this section the impact of nudging various sets of variables on nudged and non-nudged variables is analyzed.

3.1 Nudging wind and temperature

We first focus on simulations where only wind and temperature are nudged (IN-UV, IN-T, IN-UV&T, SN-UV, SN-T, and SN-UV&T), in order to have the same set of experiments for indiscriminate and spectral nudging and compare the two techniques.

Figure 2 shows the Taylor diagram for the total space–time 3-h cumulated precipitation in summer (Fig. 2a) and winter (Fig. 2b) for the simulations performed without nudging (NN with square marker) and with nudging (IN with circle marker and SN with star marker). The Taylor diagram provides a way of graphically summarizing how closely a pattern (or a set of patterns) matches the reference field (Taylor 2001). The similarity between two patterns is quantified in terms of their correlation (γ), their centered root-mean-square difference (ϵ) and the amplitude of their

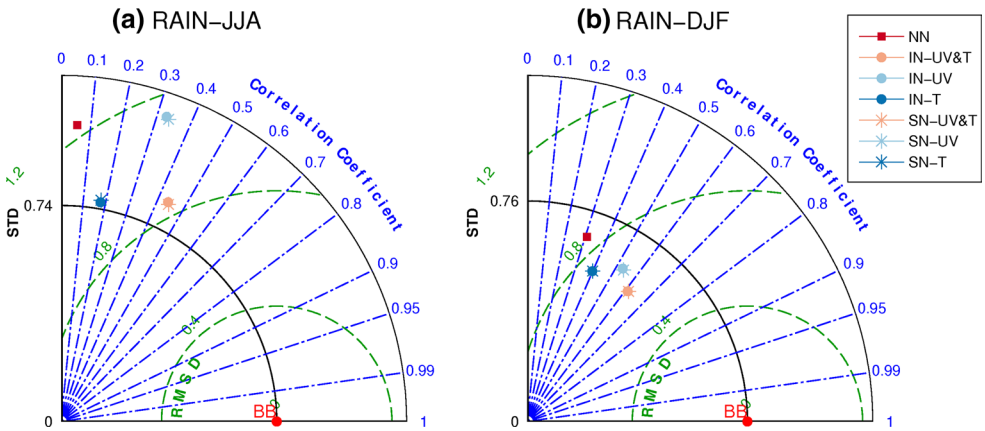

Fig. 2 Taylor diagram for daily cumulative precipitation in summer (**a**) and in winter (**b**) obtained from the LB simulations over the EURO-CORDEX domain. The *red dot* indicate the skill target for the LB simulations ("BB" stands for Big-Brother). The *stars*, *circles* and *square* display the skill scores of the SN, IN and NN simulations in the Taylor diagram, respectively

variations (represented by their standard deviations σ). Notice that we first subtract at each grid point the seasonal mean before computing the space–time standard deviation and the space–time root-mean-square difference. The LB patterns that agree well with BB are the nearest from the point marked "BB" on the x-axis. These patterns have relatively high correlation and low errors. Models lying on the arc corresponding to the standard deviation σ value of the reference have the correct standard deviation (which indicates that the pattern variations are of the right amplitude).

Overall, we note a much lower skill at reproducing the reference precipitation in summer (Fig. 2a) compared to winter (Fig. 2b). For NN simulations, the precipitation field is poorly correlated to the BB fields compared to IN and SN simulations. IN-UV&T and SN-UV&T simulations give the highest scores among all performed simulations. We also note that in summer, all simulations have systematically a higher standard deviation compared to BB, however in winter, all the simulations have a smaller standard deviation compared to BB.

Figure 3 displays maps of summer and winter precipitation bias for the different experiments. In summer, a dry bias (about 2 mm day^{-1}) over a large area of Eastern Europe is produced in the NN simulation (Fig. 3a). We

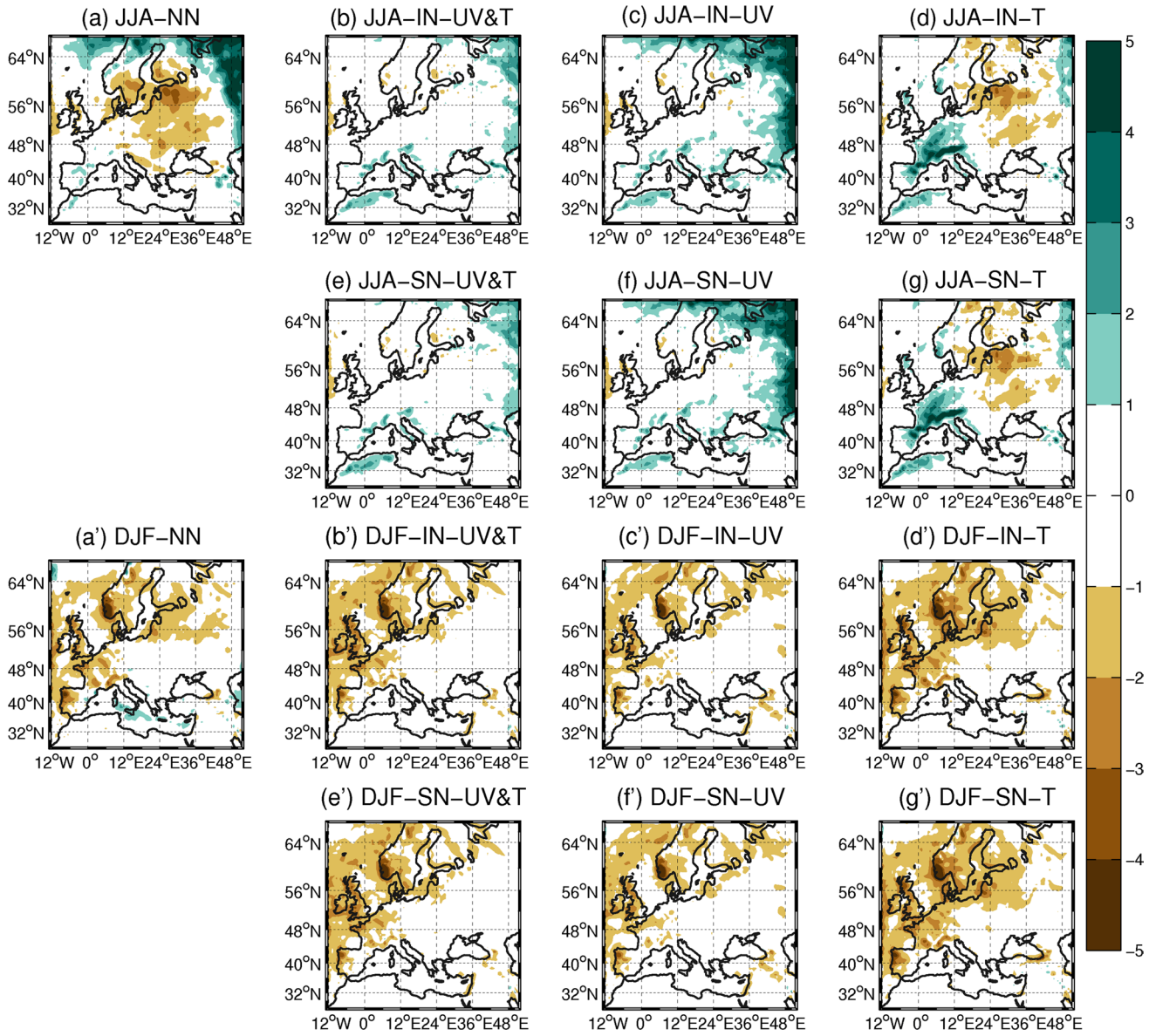

Fig. 3 The mean bias (mm day^{-1}) between the LB simulations with respect to the BB simulation of the daily precipitation for summer (**a**–**g**) and for winter (**a′**–**g′**) for NN (**a**, **a′**), IN-UV&T(**b**, **b′**), IN-UV (**c**, **c′**), IN-T (**d**, **d′**), SN-UV&T (**e**, **e′**), SN-UV (**f**, **f′**), SN-T (**g**, **g′**) simulations (see Table 2)

also note a strong wet bias over the Northeastern boundary of the domain, probably due to the resolution discontinuity between the driving large-scale fields at the domain boundaries and the fine resolution simulated field within the domain. This discontinuity causes Gibbs oscillations that are partially smoothed by applying a damping Davies zone. However, some discontinuity is unavoidable which produces strong horizontal gradient of the horizontal wind. Conservation of mass then imposes strong vertical velocities which can trigger unrealistic precipitation near the domain boundaries. Therefore, in all our diagnostics we removed the data within the Davies zone over the 5 grid points nearest to the domain boundaries. When temperature is nudged (Fig. 3d, g) this effect is significantly reduced. However, the dry bias persists. On the other hand, when only wind is nudged (Fig. 3c, f), the dry bias disappears almost completely but not the wet bias over the boundaries. It seems that the two effects are decoupled and are due to different processes. Finally, when both wind and temperature are nudged (Fig. 3b, e) the bias is strongly reduced over all the domain. In winter, precipitation is underestimated in all LB simulations and the impact of nudging is not clear.

For surface wind we found the same behavior (not shown). Nudging wind and temperature gives the highest skills.

Figure 4 is similar to Fig. 2 and shows the Taylor diagram for the total space–time surface temperature in summer (Fig. 4a) and winter (Fig. 4b) for the simulations performed without and with nudging. Again we first subtract at each grid point the seasonal mean before computing the space–time standard deviation and the space–time root-mean-square difference.

For both seasons, the NN simulations (square marker) have the lowest correlation coefficients and the highest root-mean-square error compared to the nudged simulations (IN and SN). It also has a higher standard deviation compared to the BB in summer and almost the same in winter. The nudged simulations, independently of the type of nudging (IN and SN), have the highest skills. Indeed, nudging both wind and temperature (IN-UV&T, SN-UV&T) gives the highest skills in term of correlation and root mean square. Then comes IN-UV and SN-UV simulations. Nudging only temperature shows the lowest skills among all the nudged simulations. For the same set of nudged variables it is hard to distinguish between the two nudging techniques, the circle and star markers are almost superposed.

Figure 5 shows the mean biases between the BB and LB simulations in the surface temperature in summer and winter for the not nudged (NN) simulation (Fig. 5a, a′) and the nudged simulations (IN-UV&T, IN-UV, IN-T, SN-UV&T, SN-UV, SN-T respectively Fig. 5b–g, b′–g′. In summer, the non nudged simulation displays a strong warm bias (>5 °C) over Europe and North Africa mainly over land. This bias is very weak over the sea because the sea surface temperature (SST) is prescribed from ERA-Interim reanalysis for all simulations, whereas over land, the land surface model (LSM) computes its own surface temperature. When nudging is used, this bias decreases to about ±2 °C. Here again, nudging wind and temperature show the highest skills by reducing the bias to less than ±1 °C. Unlike summer, we note a strong cold bias (about −6 °C) in winter in Eastern Europe and a smaller bias between 1 and 4 °C over almost the whole continental domain in the NN simulation. This bias is strongly reduced when nudging is applied to wind and temperature. However in winter, the impact of nudging is not as spectacular as in summer and a significant residual cold bias persists over almost the entire domain. Here again the difference between the two nudging techniques is very small. At least two facts could yield this result. The first one is that being applied above the PBL, nudging does not affect the small-scales in the PBL. Above the PBL, the small-scale structures are much less energetic so whatever its strength, nudging mainly impacts the large-scale field in LB. The second one is that the nudging time $\tau = 06\,\mathrm{h}$ is

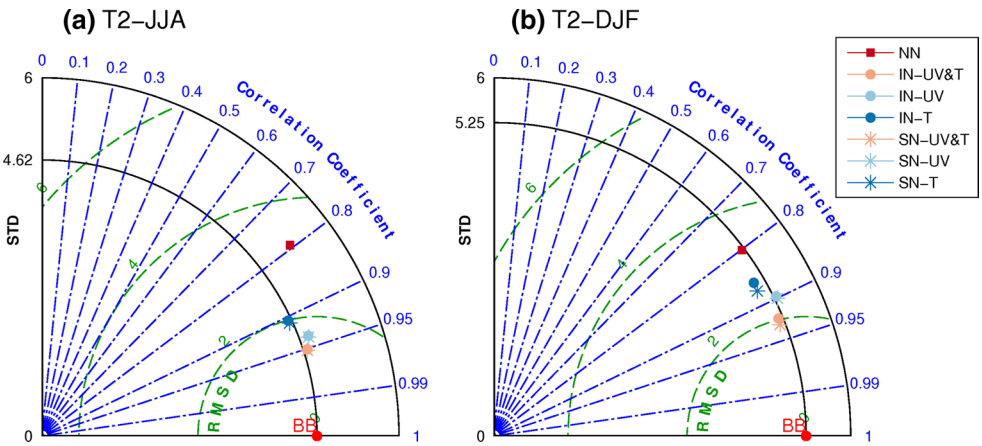

Fig. 4 Same as Fig. 2 for surface temperature

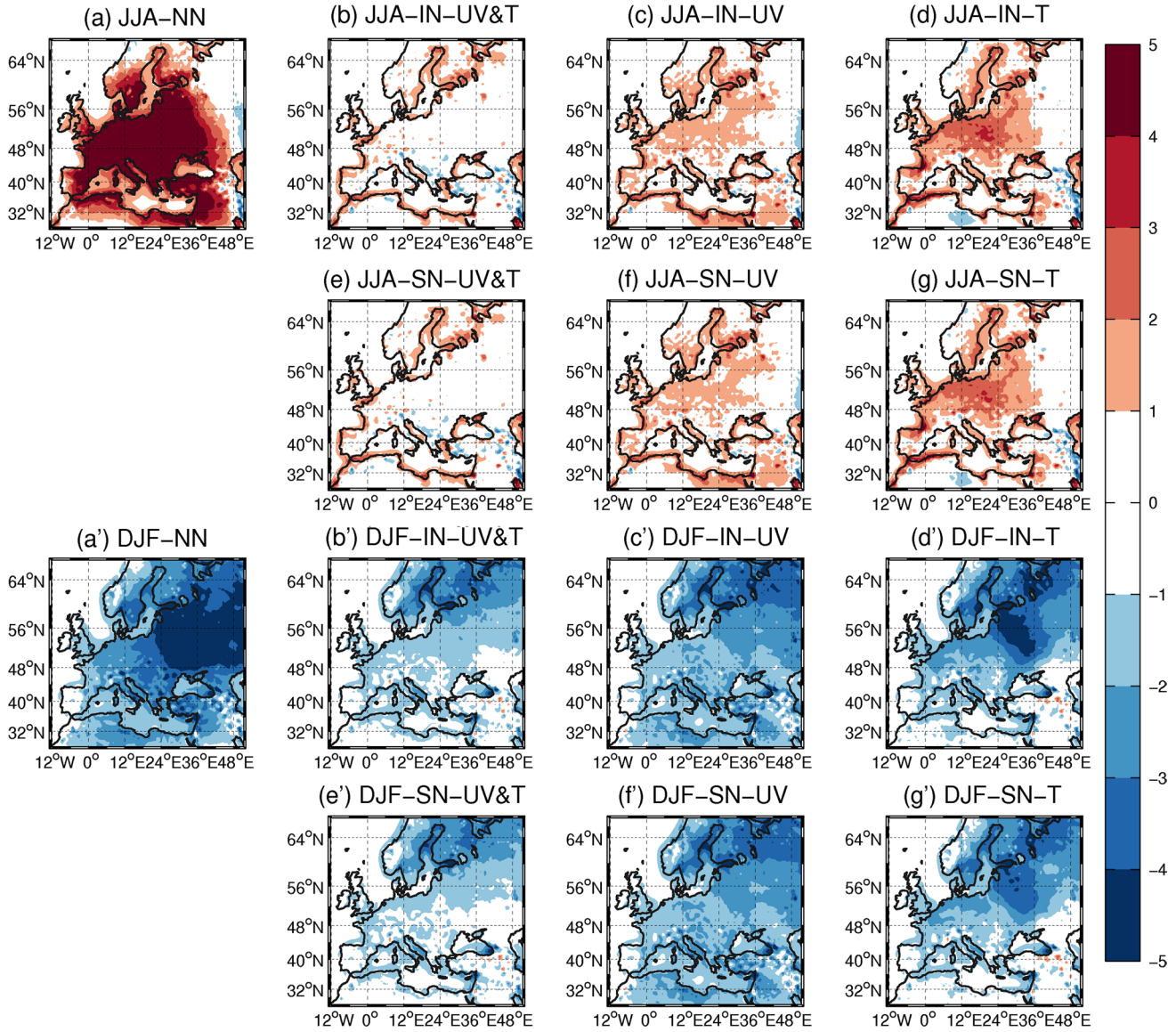

Fig. 5 Same as Fig. 3 (°C) for surface temperature (i.e. at 2 m height)

equal to its optimal value as determined in (Omrani et al. 2013). Therefore we performed additional simulations with a much smaller nudging time ($\tau = 10$ mn) and with nudging in the PBL.

Figure 6 displays the power spectra of temperature at 1,000 hPa for a relaxation time $\tau = 10$ mn and $\tau = 06$ h when nudging is applied in the PBL and above the PBL. It shows that when nudging (IN or SN) is applied above the PBL, the small-scales of the surface temperature pattern are weakly affected (panels c and d) even if the nudging coefficient is large (i.e. nudging time $\tau = 10$ mn). When nudging is applied in the PBL, the small-scales are correctly simulated when the nudging time $\tau = 06$ h and equal to its optimal value as deteremined in (Omrani et al. 2013). Conversely, the small-scales are significantly damped in IN simulation when $\tau = 10$ mn. In SN, the small-scale features of the temperature field are well reproduced in SN for length-scales smaller than the cutoff length. Overall, small scales are preserved if nudging is applied either above the PBL only or with a sufficiently long nudging time, both conditions being satisfied in our experiments, leading to small differences between IN and SN.

This large surface temperature bias produced in the NN simulations (Fig. 5a, a′) has already been observed in several studies (e.g. Radu et al. 2008; Caldwell et al. 2009; Bowden et al. 2012). Most of these studies explained this bias by an overprediction of daily-maximum temperature correlated with a low soil moisture content. As in Omrani et al. (2013), such an explanation did not hold since the very simple 5 layer land-surface model used did not

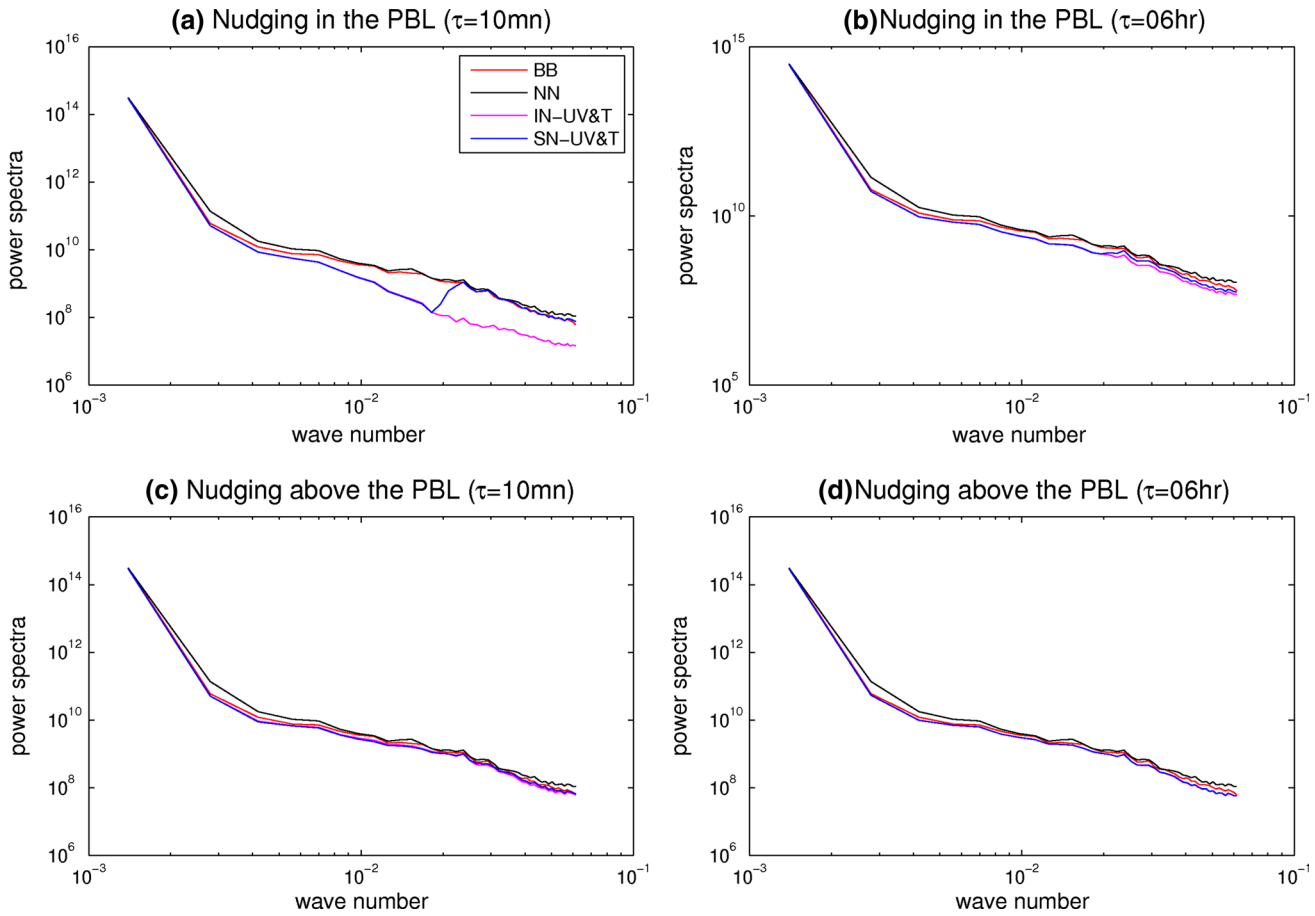

Fig. 6 Power spectra for temperature at 1,000 hPa for a relaxation time $\tau = 10$ mn (**a**, **c**) and $\tau = 06$ h (**b**, **d**) when nudging is applied in the PBL (**a**, **b**) and above the PBL (**c**, **d**)

permit to simulate soil moisture deficit. The other mechanism invoked in Omrani et al. (2013) is that the increase in temperature in summer corresponds to an atmospheric blocking situation artificially created by the model when nudging is not used. In that case small-scale discrepancies between the LB and BB can grow with time and contaminate the large scales. The NN simulation then produces in the center of the domain a large-scale atmospheric circulation which is inconsistent with the large-scale atmospheric circulation imposed at the domain boundaries and within the LB domain. This explanation is also valid in this study since the same experimental methodology is used here. We can easily verify this hypothesis. Figure 7, shows the 500 hPa geopotential height mean bias between the BB and LB simulations. The various sub-panels show the 500 hPa geopotential height mean bias for different sets of nudged variables. We note a strong positive anomaly of the summer geopotential height ($\geq$140 m) in the center of the domain for the NN simulation (Fig. 7a). When the temperature is nudged, this anomaly decreases significantly ($\leq$40 m). Whereas, when the wind is nudged, this centered positive anomaly disappears and it is replaced by a negative anomaly over the whole domain. In winter, we see on the contrary a negative bias over the Eastern Mediterranean which decreases somewhat, but not spectacularly, when the wind is nudged.

To check whether this temperature anomaly is confined to the surface or spreads over all vertical levels of the model, we plot the summer mean bias of temperature and the geopotential height at different vertical levels (900, 700, 500 and 400 hPa) for the NN, IN-UV&T, IN-UV and IN-T simulations (Fig. 8). Results for spectral nudging are not shown because we obtain very similar figures. The warm temperature bias exists at almost all vertical levels of our model when nudging is not used. Moreover, this bias is associated with a strong positive bias of the geopotential height that increases for the upper layers. Nudging reduces the temperature and the geopotential height bias at all levels ($\leq$2 °C).

These results are consistent with the results of Bowden et al. (2012) who showed evidence of a temperature bias over North America in the absence of nudging, significantly

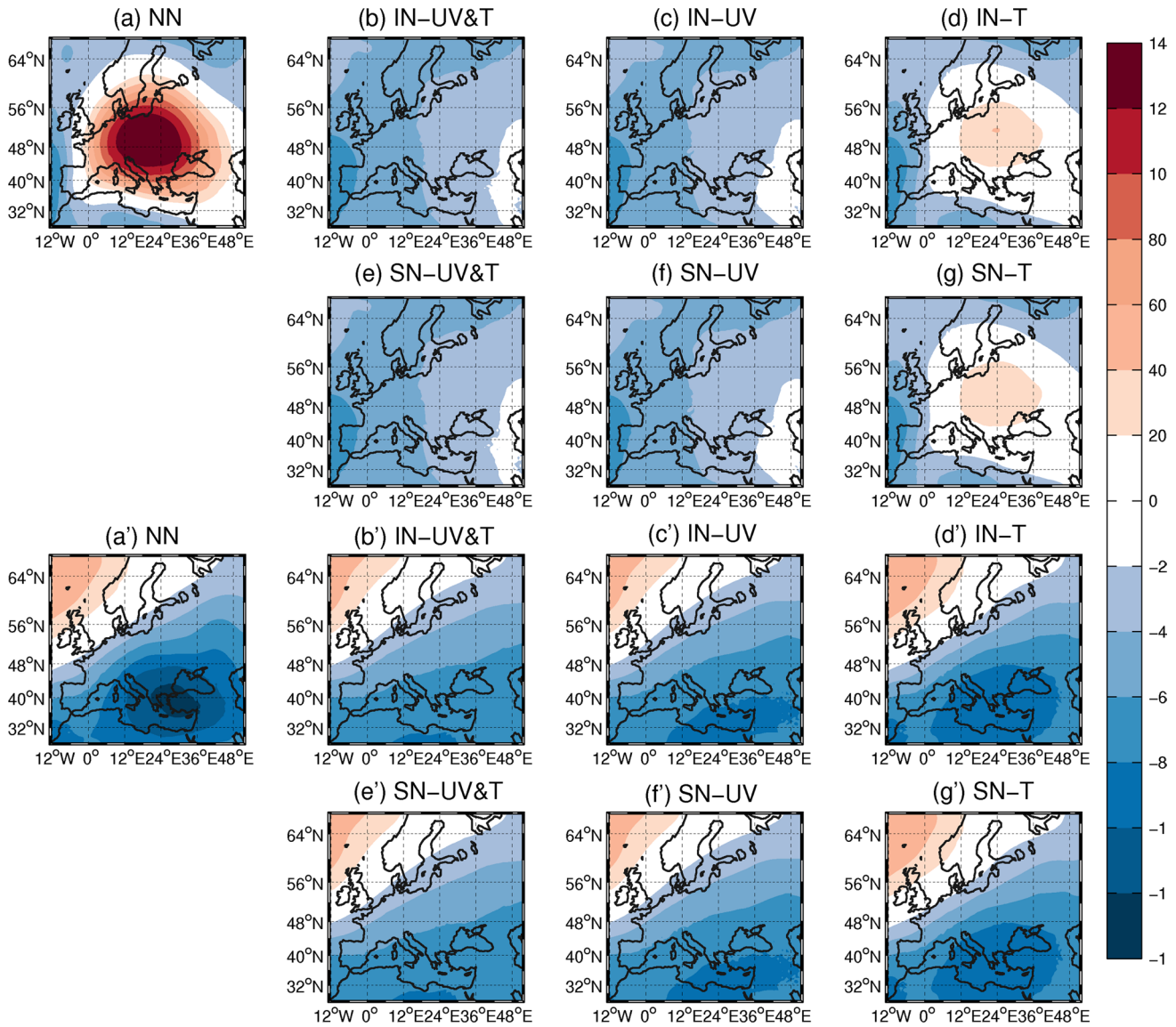

Fig. 7 Same as Fig. 5 for geopotential height at 500 hPa (m)

correlated to a 500 hPa geopotential height anomaly. The impact of the absence of nudging on the 500-hPa geopotential height, and thus on the synoptic atmospheric circulation has significant consequences on the rainfall pattern as shown in Fig. 3 (panels a and a′). In summer, the dry bias is induced in part by the positive anomaly of the 500-hPa geopotential height. The artificial high pressure over the center of the domain reduces cloud cover and precipitation producing a negative soil-moisture anomaly with smaller evaporation and higher sensible heat which in turn warms the planetary boundary layer and increases the surface temperature (Zampieri et al. 2009; Hohenegger et al. 2009).

In summer and winter, a significant residual bias on the 500 hPa geopotential height persists even when all possible variables are nudged. To analyze why, let us assume that hydrostatic balance approximately holds, which is a good approximation at scales larger than a few tens of kilometers. The temperature profile then entirely determines the pressure and density profiles, up to a constant provided by surface pressure, an independent prognostic variable in sigma-coordinate models like WRF. Now any difference in surface pressure between LB and BB contaminates the whole pressure field. This in turn affects the large-scale circulation which is approximately in geostrophic balance with the pressure field. Figure 9 displays the time-mean bias of the surface pressure. The observed pattern is remarkably similar to the mean bias in 500 hPa geopotential height. This strongly suggests that surface pressure is the missing quantity that, in addition to temperature, would allow to prevent the pressure field to diverge from its LB reference value.

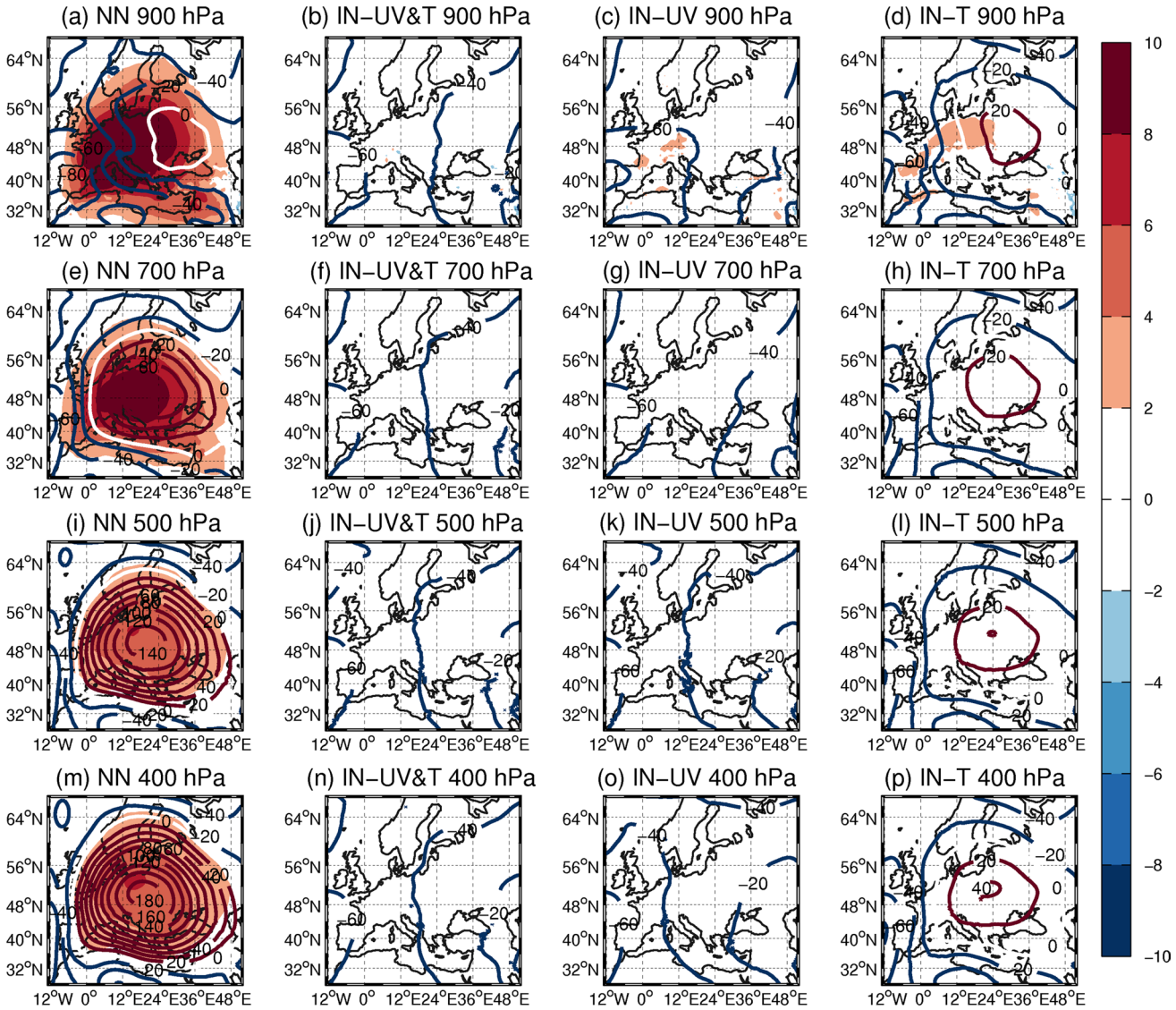

Fig. 8 The mean bias (°C) between the LB simulations with respect to the BB simulation of temperature (in *shaded color*) at 900 (**a**–**d**), 700 (**e**–**h**), 500 (**i**–**l**) and 400 (**m**–**p**) hPa for summer for NN (**a**, **e**, **i**, **m**), IN-UV&T (**b**, **f**, **j**, **n**), IN-UV (**c**, **g**, **k**, **o**), IN-T (**d**, **h**, **l**, **p**) simulations and geopotential height anomaly in contours

Figure 10 is similar to Fig. 3 but for 10m wind speed (m s^{-1}). In summer, the bias is very low over land with no significant difference between the NN simulation and the nudged ones. In winter, we note a negative bias ($\geq$3 m s^{-1}) over the Atlantic part of the domain, nevertheless weak over land. Overall, nudging has no significant effect on surface wind. Figure 11 shows the wind speed bias for different pressure levels. Near the surface the impact of nudging is not significant as shown in Fig. 10, however, for the upper level, the strong positive anomaly of the geopotential height creates an anticyclonic circulation in the center of the domain. Nudging wind remove this bias over the whole vertical level while nudging only temperature leaves a small residual bias.

3.2 Nudging moisture

We now examine the impact of nudging moisture. Note that with WRF, nudging moisture can be used only with IN. Indeed, we have compared simulations where moisture is or is not nudged, i.e. NN versus IN-Q, IN-UV&T versus IN-UV&T&Q, IN-UV versus IN-UV&Q, IN-T versus IN-T&Q. Tables 3 and 4 display the correlation coefficients and the root mean square errors between the reference (BB simulation) and the different set of experiment with and without nudging moisture for rain, temperature and wind. Overall, nudging moisture has a positive effect on rain by reducing the bias and improving the temporal variability. This effect seems to be more significant in summer than in

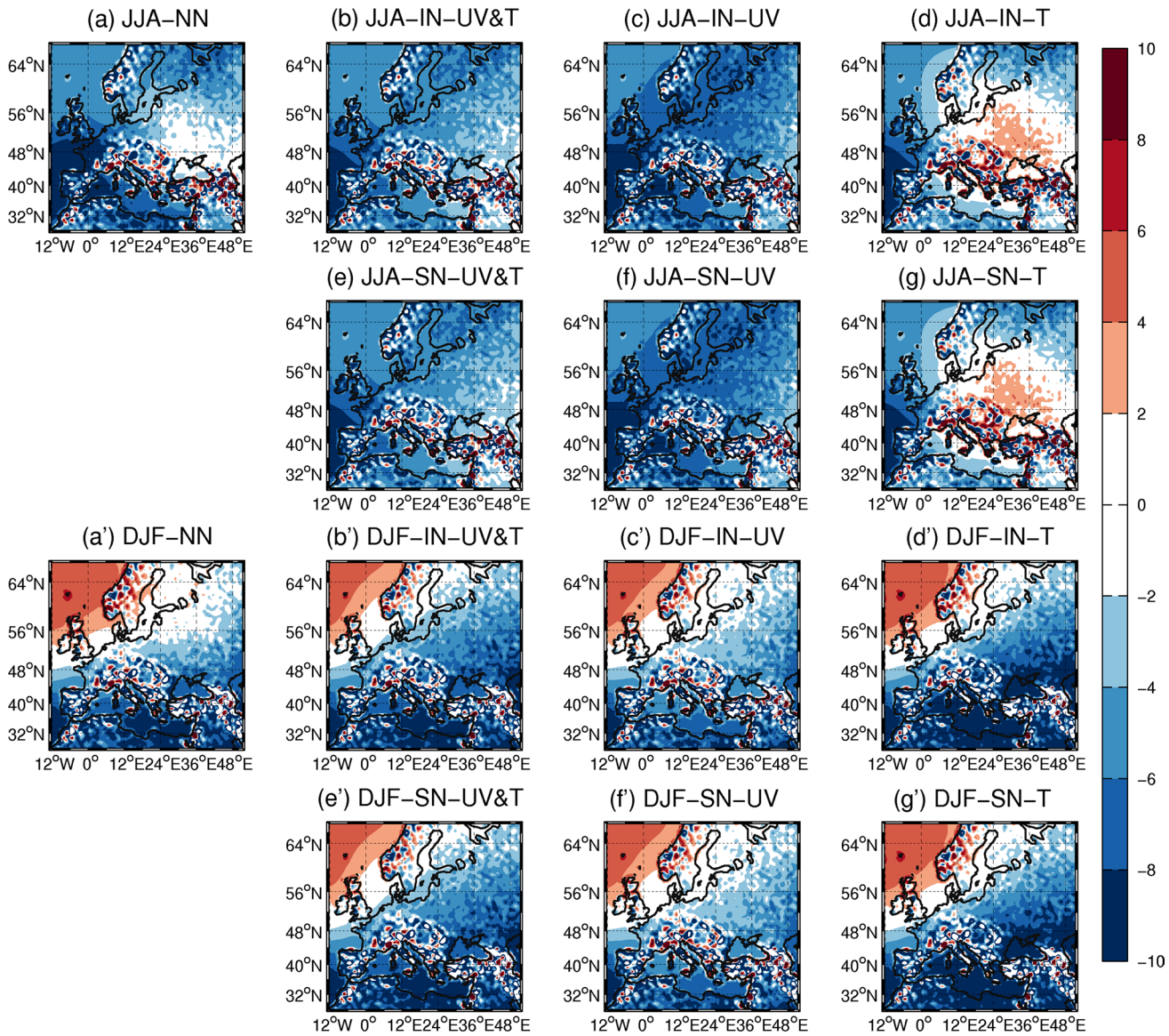

Fig. 9 Same as Fig. 5 for hydrostatic surface pressure (hPa)

winter. Indeed, it increases the correlation coefficients by 0.1 at least and reduces significantly the RMS errors. For the other variables, nudging moisture shows no significant feedback on wind or temperature. This result is consistent with the finding of Radu et al. (2008), where they compared the sensitivity of the model to the set of nudged variables and showed that nudging the specific humidity improves the rainfall but it has a weak impact on temperature. No evident reason has been found within this framework which would explain these results. The boundary layer parametrization (eg. the convection scheme) may be at stake here. However, additional investigations out of the scope of this Big Brother Experiment are left for future work.

3.3 Nudging geopotential height

The bias of the geopotential height controls a large part of the surface wind and temperature biases. Nudging the geopotential height may thus be a way to overcome the problem of the residual bias due to the surface pressure bias. With WRF, we can nudge geopotential height with SN. To identify the added value of nudging geopotential (as for moisture) we compared pairs of simulations (NN versus SN-GHT), (SN-UV versus SN-UV&GHT), (SN-T versus SN-T&GHT) and (SN-UV&T versus SN-UV&T&GHT). Results show no difference (not shown). Nudging the geopotential has no discernable effect.

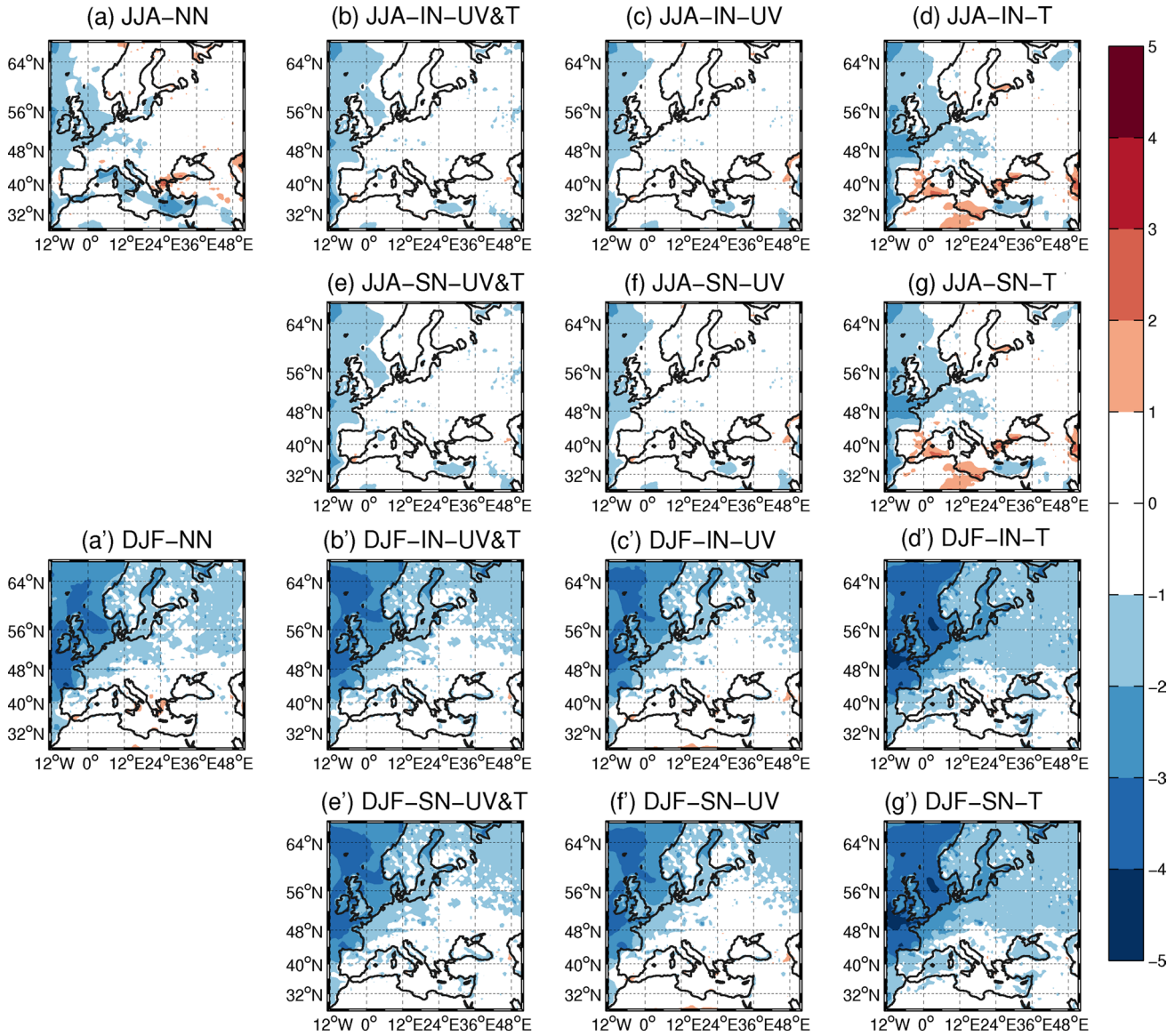

Fig. 10 Same as Fig. 3 for surface wind speed (m s^{-1})

4 Discussion: effectiveness of nudging and inter-variable relationships

We finally discuss potential dynamical causes of two observations made previously: the absence of any impact of nudging geopotential on the simulations and the persistence of a bias in surface pressure and geopotential height even when nudging wind and temperature.

4.1 Implications of a nearly-hydrostatic regime

At scales much larger than the scale height (about 10 km), non-hydrostatic effects are small. Our simulations are well within this nearly-hydrostatic regime, and we first explore implications for the biases we observed. Table 5 shows the correlation coefficient between the geopotential height bias and either the surface pressure bias ($C(\Delta\Phi_{500}, \Delta p_s)$) or the surface temperature bias ($C(\Delta\Phi_{500}, \Delta T_2)$) for NN, IN-UV&T, IN-UV and IN-T simulations, with $\Delta\Phi_{500} = \Phi_{500}^{LB} - \Phi_{500}^{BB}, \Delta p_s = p_s^{LB} - p_s^{BB}, \Delta T_2 = T_2^{LB} - T_2^{BB}$. In winter, we note that the geopotential height bias is mainly controlled by the surface pressure bias. Indeed, for the NN simulation the correlation coefficient $C(\Delta\Phi_{500}, \Delta p_s)$ is high (83.27 %) compared to $C(\Delta\Phi_{500}, \Delta T_2) = 19.23\,\%$. When we nudge the temperature (IN-UV&T and IN-T), the residual bias of the geopotential height is even more correlated to the surface pressure bias ($\geq$98 %). In summer, the geopotential bias seems to be more correlated to the

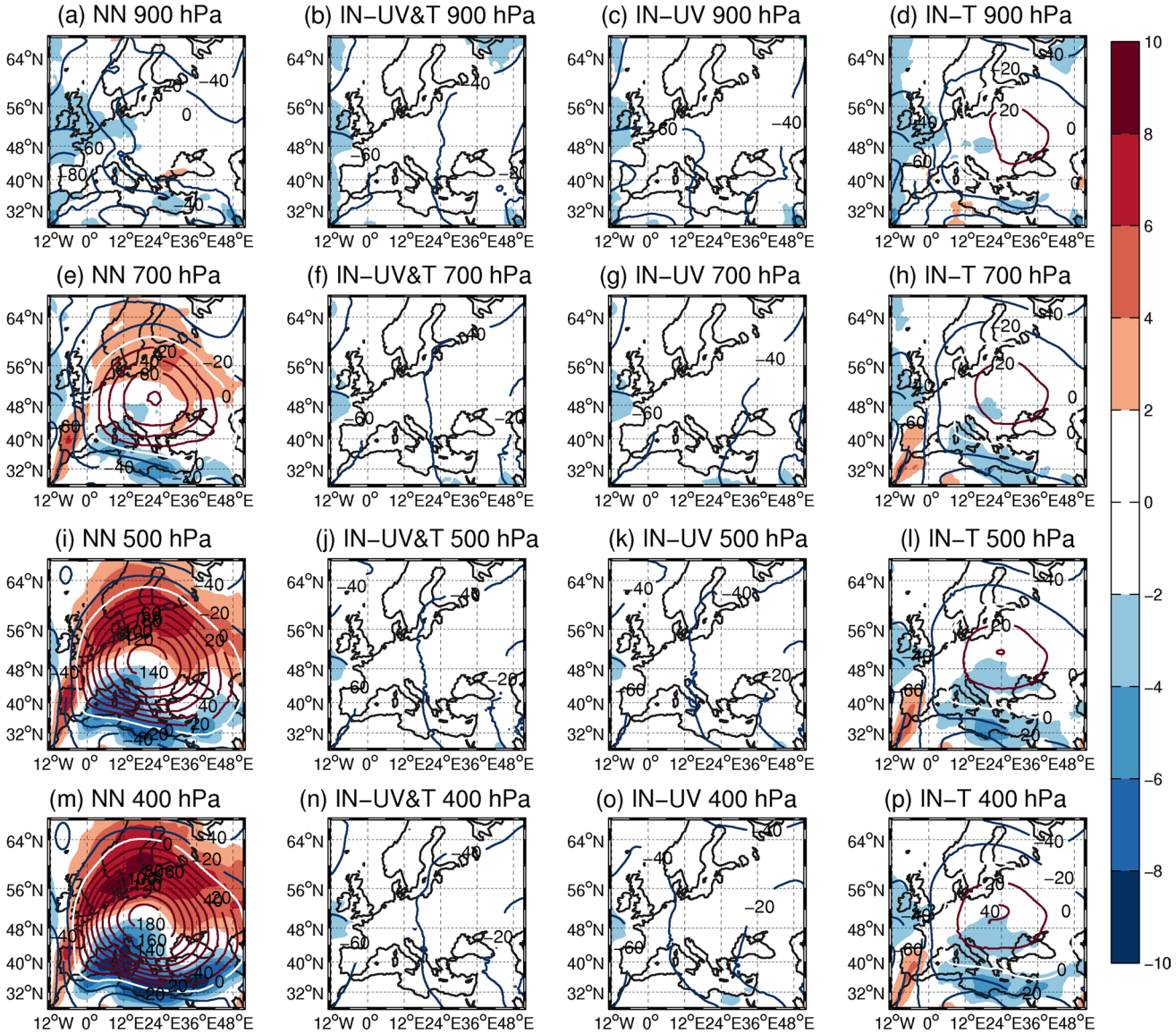

Fig. 11 Same as Fig. 8 but for wind speed (m s^{-1})

Table 3 Correlation coefficients for the different experiment set-up

	NN/IN-Q	IN-UV/ IN-UV&Q	IN-T/ IN-T&Q	IN-UV&T/ IN-UV&T&Q
Rain (JJA)	0.05/0.16	0.32/0.48	0.17/0.34	0.43/0.56
Rain (DJF)	0.30/0.48	0.53/0.69	0.39/0.55	0.61/0.72
T2 (JJA)	0.79/0.80	0.93/0.94	0.90/0.91	0.95/0.95
T2 (DJF)	0.8/0.87	0.89/0.92	0.86/0.88	0.92/0.92
U10 (JJA)	0.41/0.40	0.86/0.87	0.66/0.69	0.90/0.91
U10 (DJF)	0.69/0.73	0.86/0.89	0.77/0.79	0.91/0.92
V10 (JJA)	0.42/0.41	0.86/0.88	0.68/0.69	0.90/0.91
V10 (DJF)	0.69/0.74	0.88/0.89	0.78/0.79	0.91/0.91

temperature bias with $C(\Delta\Phi_{500}, \Delta T_2) = 84.6\,\%$ for NN simulation versus $C(\Delta\Phi_{500}, \Delta p_s) = 67.6\,\%$. When the temperature is nudged, the residual bias is strongly correlated to the surface pressure bias (~99 %).

To analyze more theoretically the results of Table 5, let us consider the hypsometric equation (Holton 1992)

$$\Phi_{500} - \Phi_s = -R\langle T\rangle ln\left(\frac{500}{p_s}\right)$$

where $\langle T\rangle$ denotes the mean temperature in the layer between the surface pressure p_s and 500 hPa and R is the gas constant for dry air ($R = 287$ J K^{-1} kg^{-1}). The corresponding geopotential height bias at 500 hPa is then:

Table 4 Root mean square error for the different experiment set-up

	NN/IN-Q	IN-UV/ IN-UV&Q	IN-T/ IN-T&Q	IN-UV&T/ IN-UV&T&Q
Rain (JJA)	1.23/0.86	1.12/0.72	0.97/0.74	0.8/0.65
Rain (DJF)	0.84/0.71	0.68/0.55	0.74/0.64	0.61/0.53
T2 (JJA)	3.22/3.20	1.68/1.57	1.99/1.91	1.46/1.36
T2 (DJF)	3.29/2.63	2.39/2.00	2.71/2.49	2.02/1.96
U10 (JJA)	3.92/3.93	1.89/1.79	2.89/2.79	1.57/1.52
U10 (DJF)	3.79/3.55	2.44/2.28	3.23/3.16	2.11/2.08
V10 (JJA)	3.91/3.96	1.86/1.76	2.82/2.74	1.56/1.50
V10 (DJF)	3.66/3.39	2.37/2.23	3.10/3.03	2.09/2.08

Table 5 Correlation coefficients between the biases of geopotential height at 500 hPa ($\Delta\Phi_{500} = \Phi_{500}^{LB} - \Phi_{500}^{BB}$), of surface pressure ($\Delta p_s = p_s^{LB} - p_s^{BB}$) and of surface temperature ($\Delta T_2 = T_2^{LB} - T_2^{BB}$)

	$C(\Delta\Phi_{500}, \Delta p_s)$		$C(\Delta\Phi_{500}, \Delta T_2)$	
	Winter	Summer	Winter	Summer
NN	0.83	0.67	0.19	0.84
IN-UV&T	0.98	0.98	0.02	0.29
IN-UV	0.89	0.82	−0.05	0.28
IN-T	0.98	0.99	0.18	0.61

Table 6 Correlation coefficient and mean bias between the geopotential height bias retrieved from respectively NN, IN-T simulations and the geopotential height computed from Eqs. 3, 4

	$\Delta\Phi_{500}^{NN,theo}, \Delta\Phi_{500}^{NN}$		$\Delta\Phi_{500}^{IN-T,theo}, \Delta\Phi_{500}^{IN-T}$	
	MJJA	NDJF	MJJA	NDJF
C	0.99	0.99	0.90	0.83
Δ	−2.13	3.79	−20.22	−19.66

$$\Delta\Phi_{500}^{theo} = \frac{1}{g_0}\left(\Phi_{500}^{LB} - \Phi_{500}^{BB}\right) = -\frac{R}{g_0}\left[\langle T\rangle^{LB} ln\left(\frac{500}{p_{LB_s}}\right) - \langle T\rangle^{BB} ln\left(\frac{500}{p_{BB_s}}\right)\right] \quad (3)$$

Table 6 shows the correlation coefficient and the mean bias between $\Delta\Phi_{500}$ and $\Delta\Phi_{500}^{theo}$ for the NN simulation. The two time series are highly correlated (99 %) with a very small bias. This confirms that the spatial scales considered here are dominated by the hydrostatic balance and the geopotential height is entirely determined by the surface pressure and the vertical profile of potential temperature. Now, if we prescribe the temperature by nudging toward the Big Brother temperature ($T^{LB} \sim T^{BB}$) Eq. (3) becomes:

$$\Delta\Phi_{500}^{IN-T,theo} = \frac{R}{g_0}\langle T\rangle^{BB} ln(500)\left[ln\left(p_s^{LB}\right) - ln\left(p_s^{BB}\right)\right] \quad (4)$$

and the geopotential bias is then, theoretically, entirely determined by the bias of the surface pressure logarithm. This is a very plausible explanation for the strong correlation coefficient between $\Delta\Phi_{500}$ and Δp_s (≥98 %) for IN-UV&T and IN-T simulations and both seasons (Table 5).

4.2 Actual degrees of freedom

To understand the absence of any impact of nudging geopotential on the simulations, it is useful to identify the actual degrees of freedom of the flow and how they relate to the prognostic variables of the numerical model. For atmospheric flows the existence of a dominant, hydrostatic balance reduces the degrees of freedom that the model can actually explore. This is especially true at the hydrostatic scales resolved in the present numerical experiments. In a hydrostatic numerical model using the same mass-based coordinate as WRF, the geopotential is a diagnostic variable which is entirely determined for each atmospheric column by the surface pressure and the vertical profile of potential temperature. When modelling hydrostatic flow with a non-hydrostatic model like WRF, it seems that geopotential is a prognostic variable but in fact it is strongly constrained due to hydrostatic balance being nearly satisfied. As a consequence nudging geopotential has a negligible effect unless the time scale for nudging is decreased until it becomes comparable to that of hydrostatic adjustment. This time is comparable to the time needed by sound waves to travel vertically over the atmospheric column, i.e. less than 1 min (Bannon 1995).

In hindsight, it is therefore entirely expected that nudging the geopotential has little usefulness. In fact nudging the geopotential should probably be avoided altogether, because it is more a diagnostic quantity than a prognostic variable. Notice that while this argument is clearly valid at horizontal scales where hydrostatic equations describe the flow well, it is probably also valid at smaller scales where the flow is non-hydrostatic. Indeed Arakawa and Konor (2009) and Dubos and Voitus (2014) have recently proposed non-hydrostatic equations where hydrostatic balance is nevertheless enforced for each atmospheric column, therefore making the geopotential explicitly diagnostic, exactly as with the primitive equations.

On the other hand hydrostatic balance puts no constraint on the value of the surface pressure, which is equivalent to the total mass of an atmospheric column. This is therefore a genuine degree of freedom. Surface pressure is associated with barotropic motion such as Lamb waves and barotropic Rossby waves. The latter play a significant role in large scale atmospheric variability at a scale of a few days (Madden 2007). It is therefore entirely possible that this mode of atmospheric motion becomes progressively inconsistent between the driving model and the driven model as time passes, if no nudging is applied. This issue might not be encountered when dealing

with small regional domains or short experiments. However for regional climate studies over large domains, nudging surface pressure may be necessary as Fig. 9 (panels c and d) suggest.

4.3 Inter-variable relationships and nudging

Nudging has been initially introduced as a data assimilation technique (Anthes 1974; Hoke and Anthes 1976; Davies and Turner 1977). When used for this purpose, nudging is typically applied during a short assimilation window (12–24 h) before a non-nudged forecast is performed. When used for the purpose of regional climate modelling, nudging is applied during the whole simulation, typically months or years. Despite this difference, it is interesting to discuss our results in the light of the understanding of nudging gained in a data assimilation context. Indeed the question of which variables can best improve a forecast when assimilated into an initial condition by nudging has been examined in some detail (Hoke and Anthes 1976; Kuo et al. 1993; Bao and Errico 1997). The general picture that emerges from these studies is that nudging a certain field can affect other fields due to inter-variable relationships imposed by the dynamics. Those relationships, which depend on the spatial scale, are captured by a normal-mode analysis of idealized models, especially the shallow-water equations (Bao and Errico1997). The latter are relevant for hydrostatic atmospheric motion because three-dimensional motion can be decomposed into vertical modes (baroclinic and external) obeying uncoupled linearized shallow-water equations.

Whenever these modes couple two fields, nudging one affects the other. For instance small-scale gravity waves have as much kinetic energy as potential energy, coupling the (divergent) velocity field and the mass field. Nudging mass only (or velocity only) will affect both mass and (divergent) velocity in that case. Indeed, although the loss of potential (resp. kinetic) energy due to nudging is partially offset by drawing energy from the kinetic (resp. potential) reservoir, the wave is damped with a damping time just twice the nudging time (detailed calculation not shown). Conversely large-scale Rossby waves have much more potential energy than kinetic energy. Nudging wind affects the mass field very weakly in that case, as the loss of kinetic energy due to nudging is compensated by drawing energy from the much larger potential energy reservoir, resulting in an overall damping time much longer than the nudging time.

Following the above reasoning, nudging the small (<Rossby radius) scales of the mass field affects mostly gravity waves, hence small-scale divergent wind. Nudging the small scales of the wind field affects both Rossby and gravity waves, the latter affecting the small scales of the mass field. Nudging the large scales of the mass field affects large-scale Rossby waves, hence large-scale wind, assuming the latter is mostly geostrophic, a reasonable assumption at midlatitudes. Nudging the large scales of the wind field affects mostly inertial waves, which have very little potential energy, so the effect on the mass field should be weak. Overall while the small-scale mass field is affected by nudging applied to wind, it is not the case of the large-scale mass field.

Translating these shallow-water results into the three-dimensional realm involves the vertical structure of normal-modes, which are either external (barotropic) or baroclinic. Baroclinic modes have a very small projection onto surface pressure while external (barotropic) modes have a vanishing temperature perturbation (Davies et al. 2003). Hence in the above intervariable relationships, mass is a synonym of temperature for baroclinic modes and of surface pressure for external modes. Especially nudging wind affects the small-scale temperature field and nudging temperature affects the large-scale baroclinic wind field. However the shallow-water analysis applied to the barotropic modes suggests that nudging temperature has no effect on wind while nudging wind effectively controls only the scales smaller than the barotropic Rossby radius (about 3,000 km). Controlling the long barotropic Rossby waves would require nudging mass, i.e. surface pressure, as suggested above. The absence of such a control opens the possibility that surface pressure becomes inconsistent with the driving field, as we have observed in our simulations.

5 Conclusion

In this work, we investigate the impact of different sets of variables nudged in regional climate simulations performed with the Weather Forcasting and Research (WRF) model in a Big Brother Experiment (BBE) framework, using indiscriminate and spectral nudging. A set of of numerical simulations has been performed over the Euro–Mediterranean region in summer and winter. We quantify statistically the ability of nudging to reduce the inconsistencies between LB and BB (reference fields) that develop over time (Omrani et al. 2012a, b, 2013).

Comparison of nudged and non nudged configurations shows that nudging clearly improves the model capacity to reproduce the reference fields from the Big-Brother simulations, regardless of the diagnosed variable. However the improvement depends on the set of variables used to nudge the regional climate simulations. The results also depend on the season and the diagnosed variable.

The tropospheric horizontal wind is by far the key variable to nudge to simulate correctly surface temperature and wind, and rainfall. To a lesser extent, nudging tropospheric temperature also contributes to significantly improve the

simulations. This is unsurprising as wind determines the transport of all conserved quantities, especially heat and moisture. These results are consistent with the study of Pohl and Crétat (2013), who showed that nudging the horizontal wind and temperature provides the best simulation of deep tropical convection with respect to observations. Furthermore wind and temperature are coupled through the thermal wind balance. Thermal wind balance follows from hydrostatic equilibrium and geostrophic equilibrium, the latter being valid at scales larger than about 1,000 km. Therefore nudging tropospheric wind or temperature directly impacts the simulation of the tropospheric geopotential height and thus the synoptic scale atmospheric circulation. Maintaining a synoptic circulation within the simulation domain consistent with the synoptic circulation at the domain boundaries is essential to avoid numerical artifacts which are known to produce large surface temperature and rainfall biases.

Nevertheless nudging wind and temperature leaves a residual bias in surface pressure and, as a consequence, in geopotential height. We suggest that this is due to the inability of the wind and temperature fields to control large-scale barotropic Rossby waves. Removing this residual bias seems to require the nudging of the surface pressure, an independent degree of freedom. This would not be without problems since nudging surface pressure actually adds a source term to the mass budget. Some care would be needed to do this in a manner consistent with the transport of potential temperature and other species.

Nudging moisture has generally a marginal impact on the quality of the regional climate simulations. However, it has a significant positive impact on the simulation of rainfall. As an immediate consequence, nudging all possible variables in WRF gives by far the best results with respect to the Big-Brother simulation. The same conclusions were found with spectral nudging and were thus not illustrated in the article. The fact that nudging can not be applied on moisture with spectral nudging in WRF (Bowden et al. 2012) is detrimental to a more thorough comparative analysis between indiscriminate and spectral nudging.

In this study, nudging has been applied to all nudged variables with the same relaxation time. Due to the different nature of the processes and scales that control temperature, wind and precipitation, the question of the use of different nudging times for wind, temperature and moisture seems relevant and should be addressed in the future. A potential limitation of this work is to be based on the single WRF model. However, for those results (ie that nudging wind and temperature has the most impact, that nudging geopotential is ineffective and that the surface pressure needs to be nudged) for which a plausible physical explanation could be found, it seems reasonable to expect that they are robust and model independent.

Acknowledgments We are thankful to R. Laprise for fruitful discussion. This research has received funding from the ANR-MEDUP project, GIS "Climat-Environnement-Société" MORCE-MED project, and through ADEME (Agence de l'Environnement et de la Maîtrise de l'Energie) contract 0705C0038. It was also supported by the IPSL group for regional climate and environmental studies. This work also contributes to the HyMeX program (HYdrological cycle in The Mediterranean EXperiment) through INSU-MISTRALS support and the Med-CORDEX program (A COordinated Regional climate Downscaling EXperiment—Mediterranean region).

References

Alexandru A, de Elia R, Laprise R, Separovic L, Biner S (2009) Sensitivity study of regional climate model simulations to large-scale nudging parameters. Mon Weather Rev 137:1666–1686

Anthes R (1974) Data assimilation and initialization of hurricane prediction models. J Atmos Sci 31:702–719

Arakawa A, Konor CS (2009) Unification of the anelastic and quasi-hydrostatic systems of equations. Mon Weather Rev 137(2):710–726

Bannon PR (1995) Hydrostatic adjustment: Lamb's problem. J Atmos Sci 52:1743–1752

Bao JW, Errico RM (1997) An adjoint examination of a nudging method for data assimilation. Mon Weather Rev 125:1355–1373

Bowden J, Otte T, Nolte C, Otte M (2012) Examining interior grid nudging techniques using two-way nesting in the WRF model for regional climate modeling. J Clim 25:2805–2823

Caldwell P, Chin HNS, Bader DC, Bala G (2009) Evaluation of a wrf dynamical downscaling simulation over California. Clim Change 95:499–521

Cha DH, Lee DK, Kuo YH (2006) An implementation of spectral nudging technique to the WRF model. In: 7th WRF users' workshop, p 7.3

Davies HC, Turner RE (1977) Updating prediction models by dynamical relaxation: an examination of the technique. Q J R Meteorol Soc 103:225–245

Davies T, Staniforth A, Wood N, Thuburn J (2003) Validity of anelastic and other equation sets as inferred from normal-mode analysis. Q J R Meteorol Soc 129:2761–2775

De Elia R, Caya D, Frigon A, Biner S, Giguère M, Paquin D, Harvey R, Plummer D (2008) Evaluation of uncertainties in the CRCM-simulated North American climate. Clim Dyn 30:113–132

Denis B, Laprise R, Caya D, Côté J (2002a) Downscaling ability of one-way nested regional climate models: the Big-Brother experiment. Clim Dyn 18(8):627–646

Drobinski P, Ducrocq V, Lionello P, the HyMeX ISSC (2009) Hymex, a potential new CEOP RHP in the mediterranean basin. GEWEX Newsl 19:5–6

Dubos T, Voitus F (2014) A semi-hydrostatic theory of gravity-dominated compressible flow. J Atmos Sci. doi:10.1175/jas-d-14-0080.1

Dudhia J (1989) Numerical study of convection observed during the winter monsoon experiment using a mesoscale two dimensional model. J Atmos Sci 46:3077–3107

Flaounas E, Drobinski P, Borga M, Calvet JC, Delrieu G, Morin E, Tartari G, Roberta T (2012) Assessment of gridded observations used for climate model validation in the mediterranean region: the HyMeX and MED-CORDEX framework. Environ Res Lett. doi:10.1088/1748-9326/7/2/024017

Giorgi F, Jones C, Asrar GR (2009) Addressing climate information needs at the regional level: the CORDEX framework. WMO Bull 58(3):175–183

Hohenegger C, Brockhaus P, Bretherton CS, Schaer C (2009) The soil moisture-precipitation feedback in simulations with explicit and parameterized convection. J Clim 22:5003–5020

Hoke JE, Anthes R (1976) The initialization of numerical models by a dynamic initialization technique. Mon Weather Rev 104:1551–1556

Holton JR (1992) An introduction to dynamic meteorology, 3rd edn. International geophysics series, vol 48. Academic Press, San Diego

Hong HMH, Juang S-Yand (1998) Implementation of prognostic cloud scheme for a regional spectral model. Mon Weather Rev 126:2621–2639

Hong SY, Dudhia J, Chen SH (2004) A revised approach to ice microphysical processes for the bulk parameterization of clouds and precipitation. Mon Weather Rev 132:103–120

Hong SY, Noh Y, Dudhia J (2006) A new vertical diffusion package with an explicit treatment of entrainment processes. Mon Weather Rev 134:2318–2341

Kain JS (2004) The Kain–Fritsch convective parameterization: an update. J Appl Meteorol 43:170–181

Kanamaru H, Kanamitsu M (2007) Scale-selective bias correction in a downscaling of global analysis using a regional model. Mon Weather Rev 135(2):334–350

Kida H, Koide T, Sasaki H, Chiba M (1991) A new approach for coupling a limited area model to a GCM for regional climate simulations. J Meteorol Soc Jpn 69:723–728

Kuo YH, Guo YR, Westwater ER (1993) Assimilation of precipitable water measurements into a mesoscale numerical model. Mon Weather Rev 127:1215–1238

Lei L, Stauffer DR, Deng A (2012) A hybrid nudging-ensemble kalman filter approach to data assimilation in wrf/dart. Q J R Meteorol Soc 138:2066–2078

Lo JC, Yang ZL, Pielke RA (2008) Assessment of three dynamical climate downscaling methods using the Weather Research and Forecasting (WRF) model. J Geophys Res 113:D09112

Madden RA (2007) Large-scale, free rossby waves in the atmosphere: an update. Tellus A 59(5):571–590

Miguez-Macho G, Stenchikov GL, Robock A (2004) Spectral nudging to eliminate the effects of domain position and geometry in regional climate model simulations. J Geophys Res 109:D13,104–D13,104

Mlawer EJ, Taubman SJ, Brown PD, Iacono MJ, Clough SA (1997) Radiative transfer for inhomogeneous atmospheres: RRTM, a validated correlated-k model for the longwave. J Geophys Res 102(D14):16663–16682

Omrani H, Drobinski P, Dubos T (2012a) Investigation of indiscriminate nudging and predictability in a nested quasi-geostrophic model. Q J R Meteorol Soc 138:158–169

Omrani H, Drobinski P, Dubos T (2012b) Spectral nudging in regional climate modeling: how strongly should we nudge? Q J R Meteorol Soc 138:1808–1813

Omrani H, Drobinski P, Dubos T (2013) Optimal nudging strategies in regional climate modelling: investigation in a Big-Brother experiment over the European and Mediterranean regions. Clim Dyn 41(9):2451–2470

Otte TL (2008) The impact of nudging in the meteorological model for retrospective air quality simulations. Part I: evaluation against national observation networks. J Appl Meteorol Climatol 47(7):1853–1867

Otte TL (2008) The impact of nudging in the meteorological model for retrospective air quality simulations. Part II: evaluating collocated meteorological and air quality observations. J Appl Meteorol Climatol 47(7):1868–1887

Pohl B, Crétat J (2013) On the use of nudging techniques for regional climate modeling: application for tropical convection. Clim Dyn 43:1693–1714

Radu R, Déqué M, Somot S (2008) Spectral nudging in a spectral regional climate model. Tellus A 60:898–910

Rockel B, Castro CL, Pielke RA Sr, von Storch H, Leoncini G (2008) Dynamical downscaling: assessment of model system dependent retained and added variability for two different regional climate models. J Geophys Res 113(D21):107. doi:10.1029/2007JD009,461

Rogers RE, Deng A, Stauffer D, Gaudet B, Jia Y, Soong ST, Tanrikulu S (2013) Application of the weather research and forecasting model for air quality modeling in the San Francisco bay area. J Appl Meteorol Climatol 52:1953–1973

Salameh T, Drobinski P, Dubos T (2010) The effect of indiscriminate nudging time on large and small scales in regional climate modelling: application to the mediterranean basin. Q J R Meteorol Soc 136:170–182

Skamarock WC, Klemp JB (2007) A time-split nonhydrostatic atmospheric model for research and nwp applications. J Comput Phys 227:3465–3485

Stauffer D, Bao J (1993) Optimal determination of nudging coefficients using the adjoint equations. Tellus 45A:358–369

Stauffer DR, Seaman NL (1990) Use of four-dimensional data assimilation in a limited-area mesoscale model. Part I: experiments with synoptic-scale data. Mon Weather Rev 118(6):1250–1277

von Storch H, Langenberg H, Feser F (2000) A spectral nudging technique for dynamical downscaling purposes. Mon Weather Rev 128:3664–3673

Taylor KE (2001) Summarizing multiple aspects of model performance in single diagram. J Geophys Res 106:7183–7192

Thatcher M, McGregor JL (2009) Using a scale-selective filter for dynamical downscaling with the conformal cubic atmospheric model. Mon Weather Rev 137(6):1742–1752

Vidard PA, Dimet FXL, Piacentini A (2003) Determination of optimal nudging coefficients. Tellus A 55:1–15

Waldron KM, Paegle J, Horel JD (1996) Sensitivity of a spectrally filtered and nudged limited-area model to outer model options. Mon Weather Rev 124:529–547

Zampieri M, D'Andrea F, Vautard R, Ciais P, de Noblet-Ducoudré N, Yiou P (2009) Hot European summers and the role of soil moisture in the propagation of Mediterranean drought. J Clim 22:4747–4758

Zou X, Navon I, Le Dimet FX (1992) An optimal nudging data assimilation scheme using parameter estimation. Q J R Meteorol Soc 118:1163–1186